Hindawi
International Journal of Polymer Science
Volume 2019, Article ID 7029143, 11 pages
https://doi.org/10.1155/2019/7029143

Research Article

The Influence of Additive Manufacturing Processes on the Performance of a Periodic Acoustic Metamaterial

John Kennedy, Lara Flanagan, Luke Dowling, G. J. Bennett, Henry Rice, and Daniel Trimble

Department of Mechanical Engineering, Trinity College Dublin, Ireland

Correspondence should be addressed to John Kennedy; jkenned5@tcd.ie

Received 8 February 2019; Revised 8 May 2019; Accepted 10 June 2019; Published 24 July 2019

Guest Editor: Jean-Philippe Groby

Advancements in 3D print technology now allow the printing of structured acoustic absorbent materials at the appropriate microscopic scale and sample sizes. The repeatability of the fundamental cell unit of these metamaterials provides a pathway for the development of viable macro models to simulate built-up structures based on detailed models of the individual cell units; however, verification of such models on actual manufactured structures presents a challenge. In this paper, a design concept for an acoustic benchmark metamaterial consisting of an interlinked network of resonant chambers is considered. The form chosen is periodic with cubes incorporating spherical internal cavities connected through cylindrical openings on each face of the cube. This design is amenable to both numerical modelling and manufacture through additive techniques whilst yielding interesting acoustic behaviour. The paper reports on the design, manufacture, modelling, and experimental validation of these benchmark structures. The behaviour of the acoustic metamaterial manufactured through three different polymer-based printing technologies is investigated with reference to the numerical models and a metal powder-based print technology. At the scale of this microstructure, it can be seen that deviations in surface roughness and dimensional fidelity have a comparable impact on the experimentally measured values of the absorption coefficient.

1. Introduction

The European COST action DENORMS (Designs for Noise Reducing Materials and Structures) has the stated goal of providing a framework for efficient information exchange, avoiding duplication of research effort, and channelling the work of groups involved towards the common goal of designing multifunctional, light, and compact noise-reducing treatments. As part of this effort, there is a need for benchmark designs and materials which can be used to cross-check and validate new numerical approaches as well as experimental measurements and manufacturing technologies. The group has recently proposed a design for a benchmark periodic metamaterial which was amenable to numerical modelling, manufacture, and experimental testing [1, 2]. This paper reports on initial results for the proposed design where the "end-to-end" process of simulation, manufacture, experimental testing, and validation was performed.

1.1. 3D Print Technology. The recent surge in metamaterial research has been facilitated by a number of advances in enabling technologies. Advances in numerical modelling also have enabled viable simulations of metabehaviour under realistic conditions. This has led to proposals for effective designs; however, until recently, these were often unrealisable. In particular, development of advanced additive manufacturing technologies has opened the door to complex geometries that are not suited to traditional manufacturing techniques. At present, there are a number of additive manufacturing technologies available and these include

(i) stereolithography (SLA)

(ii) jetting systems

(iii) direct light processing (DLP)

(iv) laser metal deposition

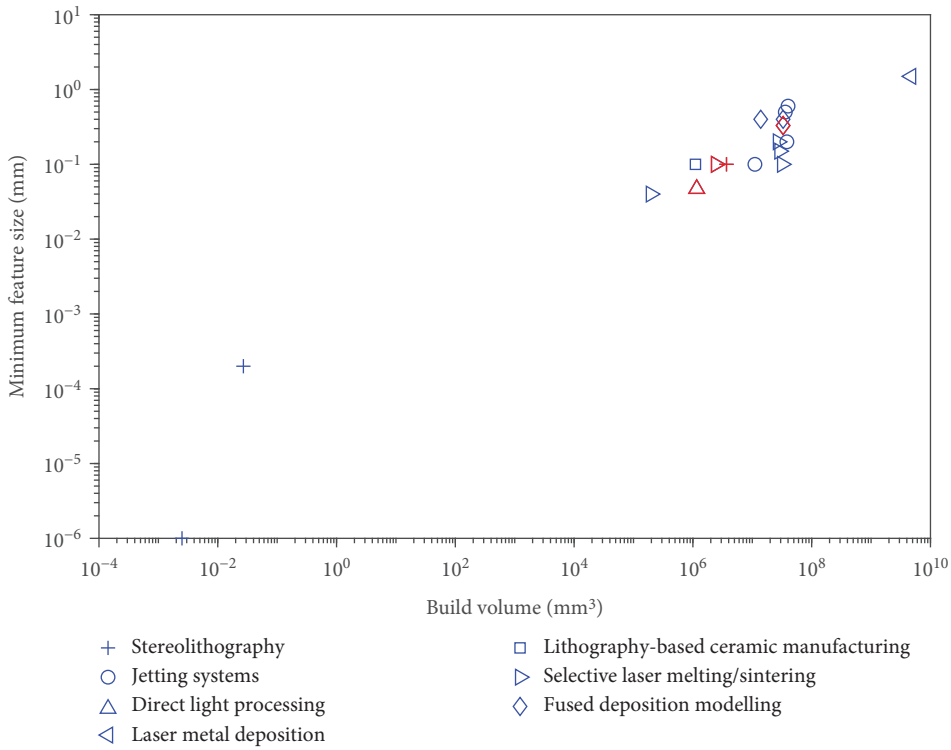

Figure 1: Build volume and minimum feature size for commercial additive manufacturing systems based on manufacturer data (the machines used in this research are identified by red symbols).

(v) electron beam melting

(vi) lithography-based ceramic manufacturing

(vii) selective laser melting/sintering (SLM)

(viii) fused deposition modelling (FDM)

The various technologies provide different capabilities in terms of resolution and build volumes. These limit the scale and quantity of the metamaterial that can be produced. The different processes also make use of different materials with FDM [3], SLA [4], and DLP [5] print technologies being based exclusively on polymers while other technologies also offer the possibility of manufacture in ceramics and metals. The design and manufacturing processes from conception through to realisation of a metamaterial is also of vital importance as is it currently unknown to what extent manufacturing tolerances or defects will impact the targeted metabehaviour. Therefore, the correct selection of the manufacturing process and assessment of the quality of the performance of the produced material are topics which require research.

A survey of the state of the art in terms of additive manufacturing technologies reveals the capabilities currently available to metamaterial researchers. The key capabilities of build volume and minimum feature size have been graphed in Figure 1. The graph shows a clear relationship between the build volume and minimum feature size and shows the overlap in the capabilities of the various technologies considered. As a general rule, an increase in build volume is matched by a corresponding increase in the minimum feature size which can be achieved. There were four printing technologies used for this research which extend from low cost desktop printers to state-of-the-art machines.

A question of interest when considering a benchmark validation material is what level of geometric accuracy and quality of surface finish is required to closely match the numerical models. A second question of interest is what is the lowest cost technology which can achieve this level of accuracy.

One of the most widely used low cost (approx. e3k) desktop printers is the FDM Ultimaker series highlighted by a red 5 on the plot. The Formlabs Form 2 is a relatively low cost SLA desktop printer (approx. e5k) highly suited to laboratory research of metamaterials as it allows a reduction of roughly one order of magnitude in minimum feature size possible over FDM machines and is highlighted with a red + on the plot. The Anycubic Photon is a very low cost (approx. e500) DLP machine and is highlighted with a red 4 on the plot.

At a fundamental level, the process of manufacturing polymers by SLA and DLP is an identical process. Both processes occur by a photomonomer reacting to light in a polymerisation reaction which results in a high level of crosslinking which generates a solid object. The source of light in each case is different. The SLA process relies on a laser light source scanning in a raster pattern. The DLP process is either a LCD screen or an array of LEDs which illuminate the entire layer at the same time. In both cases, the wavelength of light used is typically in the violet or near-UV spectrum.

The obvious difference between the use of a laser and a broad focus illumination is a dramatic difference in the

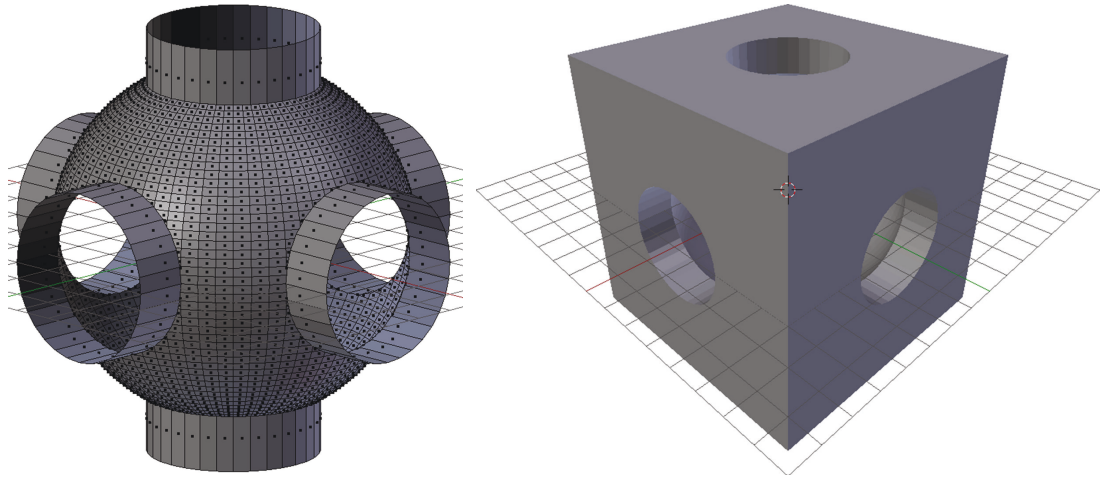

Figure 2: DENORMS benchmark design.

power density on the photopolymer. This power density difference can be a factor in the level of polymerisation that occurs and what form of reaction in the photopolymer occurs. The material used in both processes is typically an acrylic or methacrylic monomer with photoinitiators; the exact initiator and the ratio of monomer to initiator are usually proprietary information limiting the research into the area and preventing direct comparisons between the source materials.

The gaps between layers in both processes are a connection of semireacted photopolymers joining together. The polymerisation between layers can also be weaker in both technologies than those within a layer, theoretically leading to minor anisotropy. This is similar to the anisotropy found in FDM printed parts [6] but not at the same level. An effect shown in the DLP process that does not appear in SLA is the voxel effect. As the DLP process relies on pixel controlled granularity, its parts inherently have a staircase-like structure; this increases the surface roughness when compared to the smooth finish from SLA which will be more continuous in nature.

The three polymer-based print technologies have a material cost ranging from e30 (FDM) to e50 (DLP) and e170 (SLA) per kilo. The 3D Systems Prox DMP 200, highlighted by the red B symbol, is an SLM machine [7] which can print in titanium, cobalt chrome, aluminium, and stainless steel. This is a state-of-the-art machine (approx. e450k), and this work was used to manufacture in cobalt chrome at a cost of e200 per kilo of powder.

1.2. Design. The DENORMS benchmark design consists of a periodic structure of cubes with spherical internal cavities connected through cylindrical openings on each face of the cube. This design is defined by a small number of parametric features which can be varied to alter the acoustic performance of the periodic cellular material. It is also amenable to manufacture at different scales with the sphere and cylinder diameter easily varied within a cell of a given size.

In this work, a single 5 mm cubed cell size was used with fixed interior spherical cavities of radius 2.1 mm with interconnecting cylinders of radius 1 mm from all faces of the cell. These parameters were chosen in the first instance to allow for a successful manufacture of the structure in multiple print technologies. Figure 2 shows the design of the unit cell. In this work, the unit cell was used to form a lattice up to 10 layers deep and samples were made for impedance tube testing to investigate the acoustic performance.

While the DENORMS cell does not correspond closely to many of the wide range of acoustic metamaterial designs currently published in the literature, the lessons learned for the manufacture, simulation, and testing are still widely applicable to other materials. For example, recent papers on optimal sound absorber design [8], ultrathin metasurfaces [9], and space coiling metamaterials [10–12] have all utilised periodic structures realised through additive manufacturing.

There is considerable potential for acoustic metamaterials to operate at a subwavelength thickness through the use of concepts such as space coiling and labyrinthine structures. In this paper, the suitability of the DENORMS unit cell to incorporate these behaviours was also investigated through the designs shown in Figure 3. Figure 3(a) shows a labyrinthine modification to the basic structure which effectively doubles the number of resonators in a given depth, from two deep to four deep in the figure. Figure 3(b) has a mixed length design with channels of four, six, eight, and ten resonators, all contained within a depth of seven cells.

1.3. Manufacturing Considerations. Most low cost commercial 3D printers make use of fused deposition modelling (FDM) which is a 3D printing process that uses a continuous filament of a thermoplastic polymer, for example, the Ultimaker desktop printers. The resolution of these machines is potentially insufficient to accurately manufacture the spherical internal cavities and circular openings of the connecting cylinders which are included in this material's design. Additionally, these "fuzzy" internal surfaces may influence the achieved acoustic performance, potentially leading to an enhanced broadband performance [11] due to additional losses caused by the spurs. It is not a trivial task to quantify the influence of these manufacturing defects on the achieved acoustic performance of the DENORMS material; therefore, FDM samples may be unsuitable for the validation of

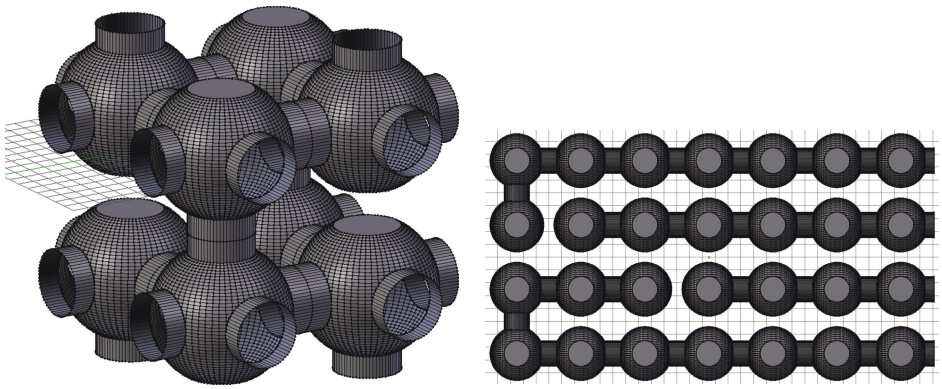

(a) (b)

Figure 3: DENORMS design variations: (a) labyrinth; (b) space coiling mixed length.

numerical codes. In this work, all FDM samples are manufactured in PLA.

The Formlabs Form 2 printer, which is based on stereolithography (SLA), can achieve a resolution which is conservatively four to ten times smaller than FDM technology while still being a low cost desktop printer. This technology uses a UV laser to cure layers of photopolymer resin with a resolution dependent on the laser spot size. It is to be hoped that the more accurate manufacturing will lead to greater agreement with the numerical simulations of the acoustic behaviour. The Anycubic Photon is a very low cost machine based on a competing technology to SLA known as digital light processing (DLP). This technology uses a UV light source and a digital LCD to cure layers of photopolymer resin by opening and closing pixels within the LCD. The resolution of the DLP printers is dependent on the pixel size in the LCD which imparts a step-like finish to the surface.

Finally, the 3D Systems Prox DMP 200, based on selective laser melting/sintering (SLM), uses a laser to form the part from a bed of metal powder. This system can achieve the smoothest surfaces with the best resolution and will be the closest to the ideal benchmark material sample. Figure 4 shows microscopy images of the four printed samples used in this work; the images were taken using a Leica S6E system under 56x magnification. The figure includes an assessment of the dimensional accuracy of the cylindrical openings and the distances between openings on the front face of the sample. The FDM prints have many defects including filaments bridging the openings and holes that are elliptical rather than circular with significant eccentricity as seen Figure 4(a). The tolerances of the other three print technologies are comparable. The surface features of the SLA and SLM technologies are related to the laser spot size and print direction. The voxel effect, unique to the DLP technology, is shown in Figure 5.

Manufacture with these four different technologies essentially introduces defects into the design which are inherent to the technology chosen. There are however significant disadvantages to all of these technologies when considering a periodic cellular design. For the SLA-based printers, the entrainment of the resin material inside the cells leads to blockages which are more difficult to remove deeper in the material. This limits the number of layers of cells which can be manufactured in a single piece. While the DLP printers suffer a similar limitation, the viscosity of the resin is generally much lower than the SLA printers and therefore easier to remove from within the part. This problem is not encountered in FDM printers as there is no excess material to be entrained inside the cells.

In this work, the Form 2 SLA printer was unable to print the DENORMS cell design to a depth of ten layers due to the entrained resin. Attempts were made to remove the entrained resin material through compressed air cleaning, ultrasonic baths, and manual evacuation. A decision was made to print the cells on the Form 2 in high resolution single and dual layers which could be combined for testing. This introduces a new complication in that it is possible to have air gaps between layers of the cells, the effect of which may be very significant on the acoustic performance. A move to selective laser melting/sintering in metals avoids all of the above issues; however, this technology can no longer be considered low cost.

In order to achieve the desired material properties, the manufactured components must be post-processed. The SLA and DLP printers use photopolymers which require additional curing under UV light following the printing process. Completed prints undergo a rigorous inspection procedure. The initial inspection is a visual inspection after print removal. This stage of inspection checks for large scale defects such as support failures, missing or damaged cells, and layer disconnects. These macro defects usually necessitate a new print or support redesign. The first quantitative check is to verify that all faces are level. This ensures that the print is not warped or twisted. It is possible that uneven curing causes the print to curl inwards on the more cured side; this is due to entrapped and entrained liquid leaving the material and causing a modest amount of shrinkage. To avoid this, prints are rotated regularly over the curing period to achieve an even curing.

The next visual inspection is to check that all corners are complete and undamaged. As some of the printing processes include a wiper passing over the print, it is possible, at the exposed corners, for a wiper crash to cause damage. The corners are also where any damage in inserting the print into the test apparatus is likely to be noticed as they are the weakest

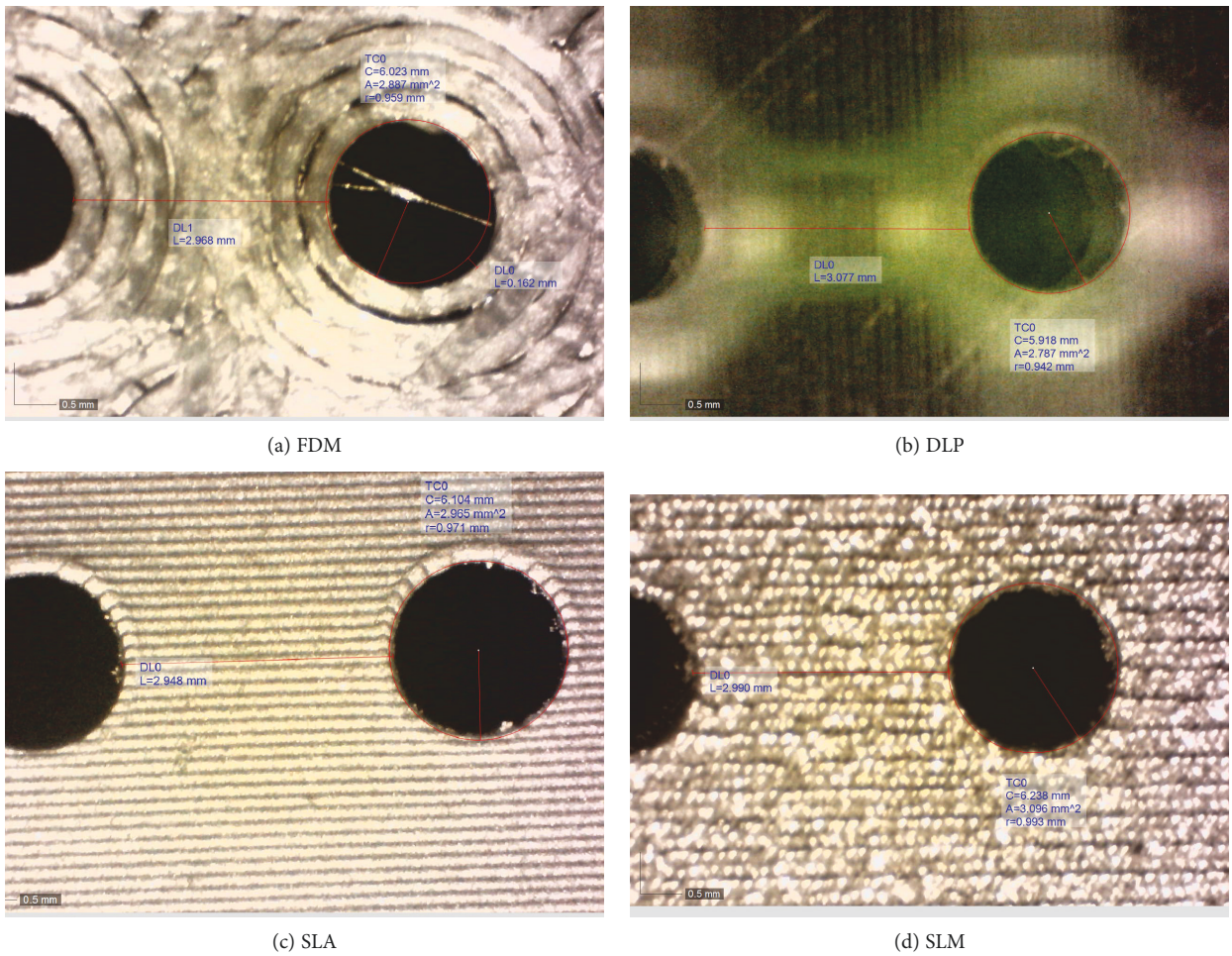

(a) FDM (b) DLP

(c) SLA (d) SLM

Figure 4: Microscopy images detailing the dimensional accuracy of the 3D print technologies.

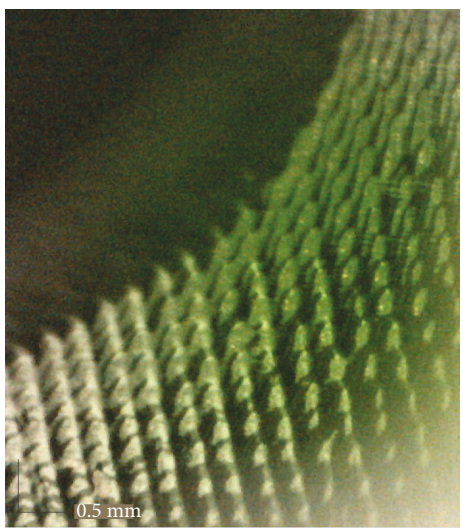

Figure 5: Microscopy image of the DLP printed components showing the voxel effect on the surface finish.

points. This weakness is due to fewer neighbouring cells being available to dissipate force without deforming. The final element of the visual inspection is to check that all designed channels are formed and clear. The DENORMS cell design has a series of cylindrical channels where air passes through. Any internal defects can usually be seen through these regular channels such as debris being embedded in the material or residue from a support spur failing into the channel.

2. Numerical Modelling

A 3D numerical model of the DENORMS cell was developed using a commercial finite element software COMSOL Multiphysics. Numerical models of the basic cell up to ten layers deep were developed in COMSOL as well as the labyrinthine and space coiling variations. The acoustic module within COMSOL 5.4 includes a full viscothermal acoustic module capable of modelling the dissipation from viscous shear and thermal conduction. However, as full viscothermal formulation comes at a high computational cost, reduced order models are often required to model complex systems [13, 14]. In this study, we restricted the analysis to full viscothermal modelling to remove any potential error associated with model simplification.

2.1. Linearised Navier-Stokes Equations. The full viscothermal acoustic model implements the linearised version of

Table 1: Properties of air used in all models.

Symbol	Value	Unit
T_0	343.2036	K
p_0	101325	Pa
ρ_0	1.2043	kg/m^3
μ	1.8140*e*-05	Pa·s
μ_b	0	Pa·s
C_p	1005.4	J/(kgK)
k	0.0258	W/(mK)

the Navier-Stokes equations. These equations are given in time harmonic form $+e^{j\omega t}$ represented by the convention $j\omega$, which solve for the acoustic pressure p, the variation of velocity field components $\mathbf{u}$, and the acoustic temperature variation T.

$$j\omega\rho_0\mathbf{u} = -\nabla p + \nabla\cdot\left(\mu\left[\nabla\mathbf{u} + (\nabla\mathbf{u})^T\right] - \left[\frac{2}{3}\mu - \mu_b\right][\nabla\cdot\mathbf{u}]I\right), \tag{1}$$

the equation of mass conservation,

$$j\omega\rho + \rho_0\nabla\mathbf{u} = 0, \tag{2}$$

and the energy equation in the frequency domain,

$$j\omega\rho_0 C_p T = \nabla\cdot(k\nabla T) + j\omega p T_0\alpha_0, \tag{3}$$

where ρ_0, μ, μ_b, I, C_p, k, and α_0 are the fluid equilibrium density, dynamic viscosity, bulk viscosity, unit tensor, heat capacity at constant pressure, thermal conductivity, and isobaric coefficient of thermal expansion, respectively. The dynamic viscosity, μ_b, is neglected and set to zero [15]. ω is the angular frequency.

The three preceding relationships are finally closed with a statement of the ideal gas law:

$$\frac{\rho}{\rho_0} = \frac{p}{p_0} - \frac{T}{T_0}, \tag{4}$$

where ρ, T_0, and p_0 are the fluid density, equilibrium temperature, and pressure, respectively.

At the fluid/solid interface, a no-slip isothermal condition is applied: $\mathbf{u} = 0$ and $T = 0$. The fluid parameters assumed in the study are listed in Table 1.

2.2. Finite Element Modelling. Within COMSOL, the equation systems were discretised using second order Lagrangian elements with quadratic shape function interpolation for the three velocity and temperature nodal variables and linear interpolation for the pressure variable [16]. The system was excited using an inlet manifold with a unit plane wave pressure excitation p_i and the depth of the manifold was 3.5 mm; the initial section is modeled using a lossless Helmholtz model with a transition to a full viscothermal model at 2 mm. And a hard backing wall was placed at the end of the series of cells.

From the average velocity reported at the inlet $\bar{u}$, a system impedance can be estimated:

$$Z = \frac{p_i}{\bar{u}}, \tag{5}$$

from which the absorptivity can be reported using

$$\alpha = 1 - \left|\frac{Z - \rho_0 c}{Z + \rho_0 c}\right|^2, \tag{6}$$

where c is the sonic speed:

$$c = \sqrt{\frac{\gamma P_0}{\rho_0}}, \tag{7}$$

and the ratio of specific heats γ is set at 1.41.

The viscothermal model requires special attention to meshing near the boundaries. Kirchoff [17] and Rayleigh [18] provided solutions for sound propagation through infinitely long narrow tubes and determined frequency-dependent boundary layer thicknesses based on the following:

$$\delta_{visc} = \sqrt{\frac{2\mu}{\omega\rho_0}}$$
$$\delta_{therm} = \sqrt{\frac{2k}{\omega\rho_0 C_P}} \tag{8}$$

In air, the Prandtl number is the ratio of these penetration depths $P_r = \delta^2_{\text{visc}}/\delta^2_{\text{therm}}$ and is ~0.7. [19] which enables the viscous boundary layer to be used as a meshing control parameter at the boundaries. For the largest space coiling system, this was set using automatic boundary layer settings under COMSOL, and absorptivity results were compared to user-specified boundary layer thicknesses at every 500 Hz step. It should be noted that (expected) surface roughness will increase the acoustic boundary layer thicknesses [20] and thus have an effect on the absorptivity, but this increase was not modelled in this paper as no definitive roughness measurements were available. In general, a five element per wavelength with the parameterised boundary layer meshing is the default setting used by COMSOL. However, in the case of the largest space coiling system, this was reduced by increasing the maximum element size parameter (2.1 mm) for viable run times. A number of convergence studies showed the reported absorptivity to be relatively insensitive to further refinement. Depending on the system being considered, half or quarter section symmetries were also taken advantage of to reduce model size. For the other models, a quarter section was used. The maximum element size was kept at five elements per wavelength, and boundary layer thicknesses were changed for every 500 Hz increment.

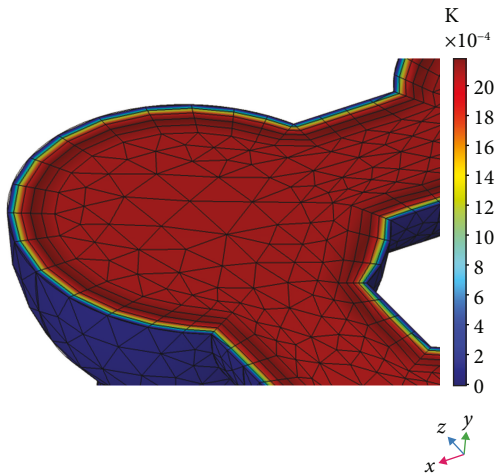

Figure 6: Temperature variation (K) unit cell at $f = 500$ Hz.

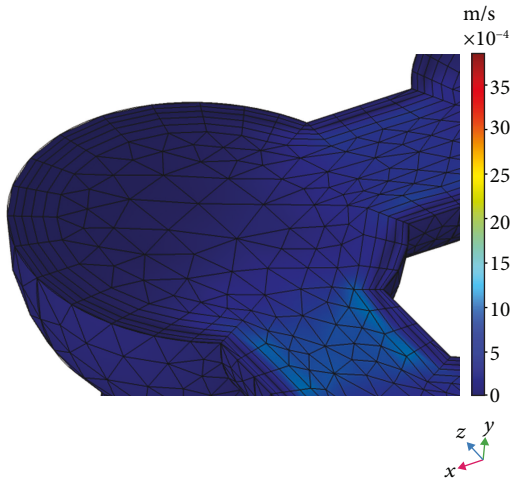

Figure 7: Axial component of velocity (m/s) unit cell, at $f = 500$ Hz.

In addition, Padé-based frequency sweeps were availed of to deliver a resolution of 50 Hz for the mixed length space coiling and 10 Hz for the other models with run times of 24 hours using a modest workstation (Xeon CPU 14 Core, 2.6 GHz, and 64 Gb RAM).

The mesh structure for some sample temperature and velocity plots at 500 Hz are presented in Figures 6 and 7.

3. Experimental Testing

The primary lab-based acoustic validation of the material performance is the measurement of the complex surface acoustic impedance leading to an absorptivity α. This can also be compared with the numerical predictions using the methods described above.

The measurements used here all followed the ISO 10534-2:2001 which describes the test rig and procedures for estimating the complex acoustic impedance of a material under normal incidence using the two-microphone or transfer function method. This leads to an estimate of the reflection

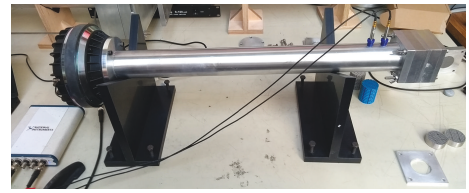

Figure 8: Impedance tube rig.

coefficient R at the target surface which then yields the absorptivity coefficient α from

$$\alpha = 1 - |R|^2, \tag{9}$$

which is completely analogous to equation 6. Values of the α absorption coefficient vary with frequency and range between 0 and 1, with 1 representing complete absorption.

In these tests, the sample is placed in an impedance tube and is backed by a hard, reflective termination. A custom rig, shown in Figure 8, with a 40 mm internal diameter was used for these tests with an upper frequency limit of 4000 Hz. The lower limit is determined by the speaker and is in the region of 300 Hz. On the left hand side of Figure 8, we can see the BMS 4591 speaker which is driven by the output signal of a National Instruments DAQ which has been amplified by a power amplifier. The speaker bolts on to the end of the tube to provide a tight seal with little leakage of sound. The square section on the right of Figure 8 is the sample holder which opens to hold cylindrical samples of 40 mm diameter up to 50 mm deep. In the experimental rig, the hard termination is provided by a 20 mm thick piece of aluminium which can be bolted on the end of the tube.

GRAS 40PL array microphones were chosen to instrument the rig as they have a frequency response (±1 dB) in the region of 50 Hz–5 kHz and upper limit of the dynamic range of 142 dB re 20 μPa allowing for testing up to high pressure amplitudes. The microphones are connected to the National Instruments DAQ, and the signals were recorded using a MATLAB interface. The microphones were calibrated using the switching methods described in ISO 10534-2:2001.

During the test procedure, band-limited white noise at 90 dB was presented through the speaker and the sound pressures were measured by the two microphones. In this work, the resulting spectral resolution of the tests was 2 Hz with 1000 averages used for the estimation of the frequency response functions required to generate R and Z. All measurements were repeated three times with complete dismounting of the sample between measurements to insure repeatability of the test procedure.

The reflection and absorption coefficients are also affected by factors such as porosity and surface finish of the material. If the material is compressible, energy can also be lost to internal friction in the material as it is loaded and unloaded by the incident pressure wave. In addition, material thermal conductivity may account for further losses. These additional losses will be influenced by both the print quality and material used in the manufacture.

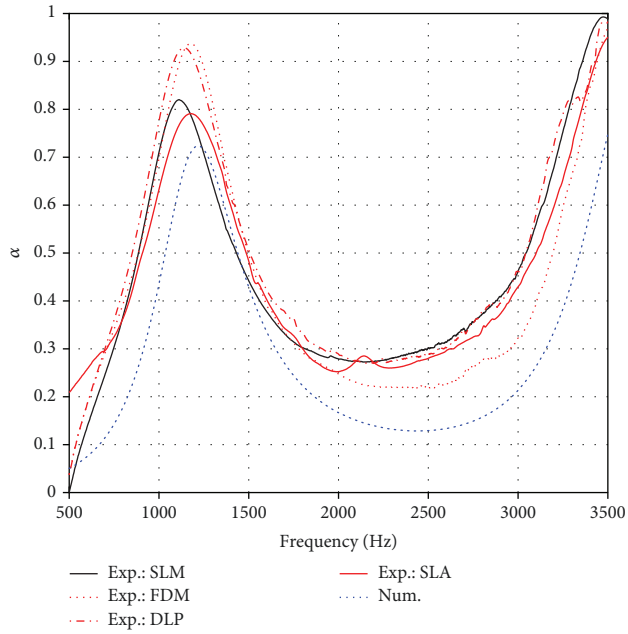

Figure 9: Absorption coefficient for four different prints of the 10-layer-deep DENORMS cell.

4. Results

Figures 9–13 report the experimental and numerical results for the cases considered. The results for the baseline ten-layer-deep design are shown in Figure 9. From all four prints, there is a double peak in the absorptivity in the regions of 1150 Hz and 3500 Hz. Experimentally, the results for the cobalt-chrome SLM sample produced using the 3D Systems machine is considered the best standard of geometric accuracy and surface finish, and this is shown as a black line in the figure. The three low-cost polymer-based experimental results are shown in red on the plot. The full viscothermal numerical model is plotted in blue. The numerical model underpredicts the absorption across the full frequency range, a fact most likely related to the lack of any surface roughness considerations in the numerical approach. The same colour conventions are used for subsequent plots.

There is good agreement between the SLM sample and the SLA sample produced on the Form 2 for the location and amplitude of the first peak. The FDM and DLP prints, manufactured on the Ultimaker and Photon machines, produce peaks in the absorption at roughly the same frequency but at high amplitudes. The increase in absorptivity can likely be attributed to the remaining spurs and low quality surface finish of the sample introducing additional losses within the channels. For the DLP technology, the increase in absorption may be attributed to the increased surface roughness due to the voxel effects which prevent as smooth a finish as the SLA and SLM technologies. The numerical model underpredicts losses as it assumes a completely smooth surface. An allowance for surface roughness by adjustment, for example, of the viscosity to model the thicker boundary layers would move these plots closer particularly to the SLM and SLA data.

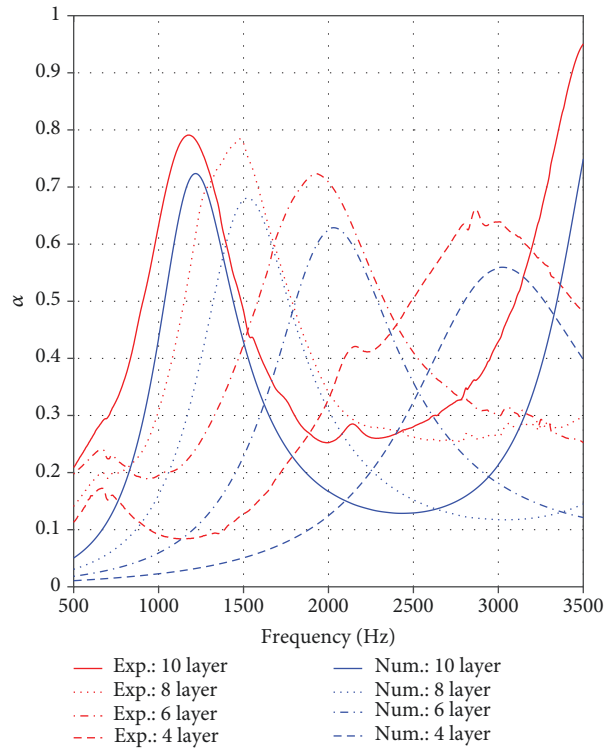

Figure 10: Absorption coefficient for 4, 6, 8, and 10 layers deep of the DENORMS cell printed on the SLA Form 2 (red: experimental results; blue: numerical results).

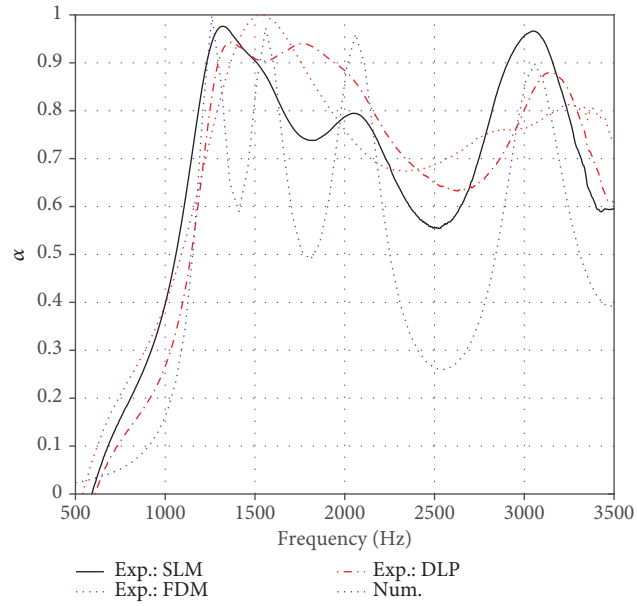

Figure 11: Absorption coefficient for combined 4-, 6-, 8-, and 10-layer depths of the DENORMS cell.

It appears from these results that any errors associated with the manual positioning of the SLA polymer disks are of less importance than the quality of the interior geometry, and from this, we can conclude that the Form 2 may be a viable, low cost system suitable for producing a sample for comparison to numerical models. The divergence

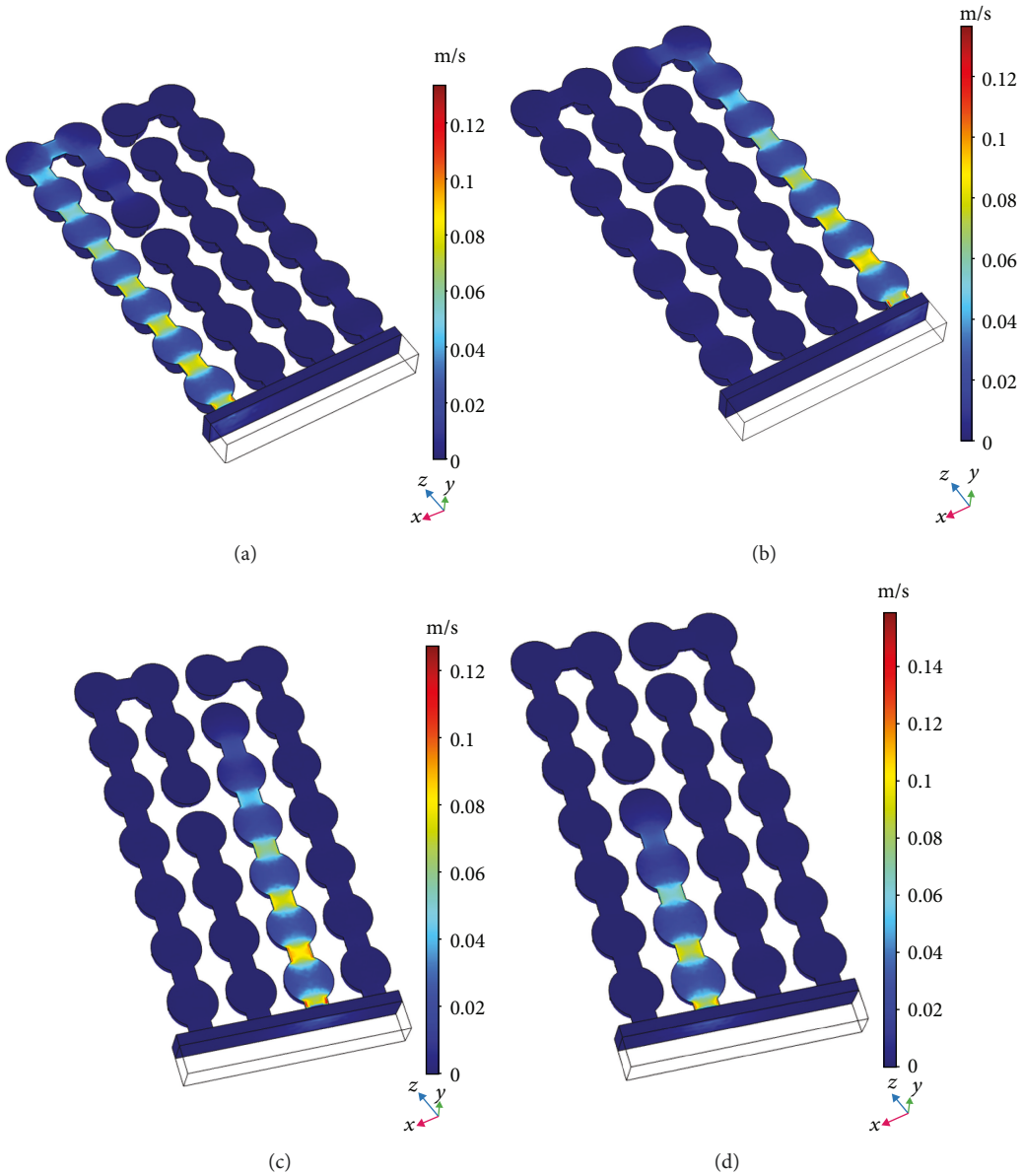

Figure 12: Axial component of velocity (m/s) within the lattice: (a) $f = 1250$ Hz; (b) $f = 1550$ Hz; (c) $f = 2050$ Hz; (d) $f = 3050$ Hz.

of the Ultimaker samples from the 3D systems sample is likely too great to allow it to be used for validation purposes. As the DLP technology improves through increased pixel count and variable exposure times, the voxel effect will reduce and it may therefore become a lower cost alternative to the SLA and SLM print technologies.

Due to the necessity to limit manufacture to single and dual layer disks on the Form 2, it was also possible to test other combinations of disks to produce different numbers of layers. Figure 10 reports the experimental and numerical results for four, six, eight, and ten layers deep. A same trend can be seen in the location and magnitude of the peaks. As the number of layers decreases, the location of both peaks shift to higher frequencies and the magnitude of the absorptivity drops with the numerical model under predicting absorbency and shifting slightly higher in frequency. This result provides the inspiration for the mixed length design as a combination of lengths is likely to provide a broadband absorption as these separate resonant peaks merge.

Figure 11 reports the experimental and numerical results for the 10-8-6-4 mixed length samples. The samples were produced using SLM, DLP, and FDM technologies. An SLA sample could not be produced using the Form 2 as the resin viscosity was too high for the entrained resin to be removed from within the sample. The numerical model produces a good estimation of the combination behaviour of the design; however, it assumes fully vacated cross-channels and smooth surfaces neither of which existed in the manufactured samples. Distinct peaks are thus reported and are confirmed by the peak frequency snapshots of the acoustic velocity at 1250 Hz, 1550 Hz, 2050 Hz, and 3050 Hz as shown in Figure 12. The behaviour of the FDM-produced sample is different to that predicted by the numerical model, and there is a more broadband behaviour without clear resonant peaks.

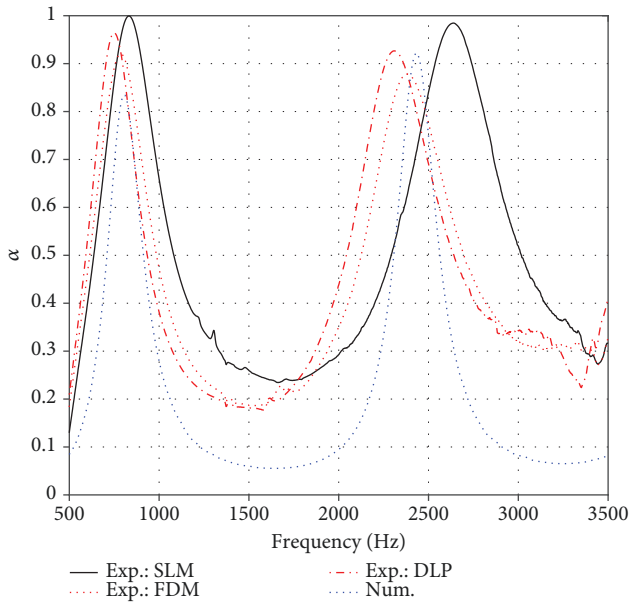

Figure 13: Absorption coefficient for a 10-layer depth of the labyrinth DENORMS cell (equivalent to a 20-layer depth).

The DLP and SLM samples have a close match to the numerical predictions, and the locations of multiple resonant peaks are visible within these experimental results. This design has achieved relatively high broadband absorption with a low thickness of 35 mm.

The final results shown are the experimental and numerical results for the labyrinthine concept. In this case, the "S"-shaped path of the resonators doubles the number of cavities within a given depth. The cross-linking side branches were required in order to allow the resin to be removed from the DLP sample and aid the removal of metal powder from the SLM sample. In this instance, there was a partial failure of the SLM sample which led to a slight eccentricity in the sample necessitating some post-processing to insure a clean fit inside the sample holder. Due to time and financial constraints, a second sample could not be produced.

The SLM, FDM, and DLP samples have similar locations for the frequency of the first peak in absorption, but the SLM sample deviates for the frequency of the second peak. This deviation may be the result of the original eccentricity in the print. In this case, the numerical model again captures well the location and amplitude of the peaks in the absorption coefficient.

5. Conclusion

This work has reported on the design of a periodic acoustic metamaterial that is suitable for use as a benchmark validation case. The design was realised through four different additive manufacturing technologies which ranged from low cost desktop printers to state-of-the-art machines. While all print technologies provide a reasonable match to the numerical results, there are deviations which are clearly due to geometric tolerances and surface roughness which become more pronounced in geometries where cross-channels may become difficult to clear after manufacture. Three polymer-based print technologies were investigated, namely, FDM, DLP, and SLA. Experimentally, the SLA sample was closest to the high quality SLM sample produced in cobalt-chrome. This demonstrates the potential of the SLA technology to accurately produce complex interior geometries with a smooth surface finish. Both the SLA and SLM samples were in very close agreement with the numerical models in terms of the locations of the peaks in absorption. The SLA and SLM samples still had a generally higher absorption value than was predicted numerically possibly due to their surface finish.

These results indicated that the manufacture of a benchmark validation material may be possible at relatively low cost using the current polymer-based SLA technologies. However, there is considerable difficulty in using this technology with designs resulting in large quantities of entrained resin as these become difficult to remove.

The use of a FDM Ultimaker printer highlighted the potential for low quality prints to significantly influence the achieved performance; this is considered an obstacle for the production of validation data using this type of printer technology should designs at the fineness of scale required to induce significant flow resistivity be attempted. The DLP printer was capable of producing geometrically accurate samples, but there was evidence to suggest that the increased roughness over the SLA samples due to voxel effects led to increased levels of absorption. The DLP technology is a promising approach for the production of very low cost validation materials in polymers.

Clear trends as a function of depth were identified in the experimental and numerical results. The results were the inspiration for two modifications to the design to incorporate both space coiling and labyrinthine elements. These modifications successfully demonstrated increased broadband behaviour and the ability to shift the resonant behaviour to a lower frequency for the same sample thickness. The DENORMS design is therefore highly suitable for use as a benchmark and validation tool in the development of acoustic metamaterials.

The current scale of the design is at the limit of the low cost additive manufacturing technologies, but finer scales can readily be achieved in the state-of-the-art machines. The viscosity of the DLP and SLA polymer resins poses a significant challenge to producing finer scale parts using these technologies. The lower viscosity of the DLP resin allows for easier extraction of the entrained material in samples at the scale produced here.

Data Availability

The CAD design and absorption coefficient data used to support the findings of this study are included within the article.

Conflicts of Interest

There are no conflicts of interest with this research or the data presented herein.

Acknowledgments

This work was partially funded through the AERIALIST project no: 723367 EU H2020-EU.3.4. Societal Challenges Smart, Green And Integrated Transport. The authors wish to acknowledge the COST Action DENORMS (CA 15125) and in particular Dr. Tomasz G. Zielinski, Department of Intelligent Technologies, Institute of Fundamental Technological Research of the Polish Academy of Sciences, who proposed the design of the unit DENORMS cell. The authors wish to acknowledge the AMBER Additive Research Lab in facilitating the manufacturing of our metal test specimens and the AR Lab staff on providing training and guidance on the manufacturing process. The AR Lab has been enabled by a €3.3M award from the Science Foundation Ireland as part of their research infrastructure program and an additional €1M investment from the European Research Council.

References

[1] K. C. Opiela, M. Rak, and T. G. Zielinski, "A concept demonstrator of adaptive sound absorber/insulator involving microstructure-based modelling and 3Dprinting," in *Proceedings of ISMA2018 Including USD2018*, Leuven, Belgium, September 2018.

[2] L. Flanagan, H. Rice, D. Trimble, L. Dowling, and J. Kennedy, "The use of a benchmark periodic metamaterial to inform numerical modelling and additive manufacturing approaches," in *Proceedings of ISMA2018 Including USD2018*, Leuven, Belgium, September 2018.

[3] S. H. Masood, "Intelligent rapid prototyping with fused deposition modelling," *Rapid Prototyping Journal*, vol. 2, no. 1, pp. 24–33, 1996.

[4] M. N. Cooke, J. P. Fisher, D. Dean, C. Rimnac, and A. G. Mikos, "Use of stereolithography to manufacture critical-sized 3d biodegradable scaffolds for bone ingrowth," *Journal of Biomedical Materials Research Part B: Applied Biomaterials*, vol. 64, no. 2, pp. 65–69, 2003.

[5] I. Cooperstein, M. Layani, and S. Magdassi, "3d printing of porous structures by UV-curable O/W emulsion for fabrication of conductive objects," *Journal of Materials Chemistry C*, vol. 3, no. 9, pp. 2040–2044, 2015.

[6] S.-H. Ahn, M. Montero, D. Odell, S. Roundy, and P. K. Wright, "Anisotropic material properties of fused deposition modeling abs," *Rapid Prototyping Journal*, vol. 8, no. 4, pp. 248–257, 2002.

[7] M. Agarwala, D. Bourell, J. Beaman, H. Marcus, and J. Barlow, "Direct selective laser sintering of metals," *Rapid Prototyping Journal*, vol. 1, no. 1, pp. 26–36, 1995.

[8] M. Yang, S. Chen, C. Fu, and P. Sheng, "Optimal sound-absorbing structures," *Materials Horizons*, vol. 4, no. 4, pp. 673–680, 2017.

[9] Y. Zhu, X. Fan, B. Liang, J. Cheng, and Y. Jing, "Ultrathin acoustic metasurface-based Schroeder diffuser," *Physical Review X*, vol. 7, no. 2, article 021034, 2017.

[10] R. Ghaffarivardavagh, J. Nikolajczyk, R. Glynn Holt, S. Anderson, and X. Zhang, "Horn-like space-coiling metamaterials toward simultaneous phase and amplitude modulation," *Nature Communications*, vol. 9, no. 1, article 1349, 2018.

[11] C. Chen, Z. Du, G. Hu, and J. Yang, "A low-frequency sound absorbing material with subwavelength thickness," *Applied Physics Letters*, vol. 110, no. 22, article 221903, 2017.

[12] Y. Xie, B.-I. Popa, L. Zigoneanu, and S. A. Cummer, "Measurement of a broadband negative index with space-coiling acoustic metamaterials," *Physical Review Letters*, vol. 110, no. 17, article 175501, 2013.

[13] H. Tijdeman, "On the propagation of sound waves in cylindrical tubes," *Journal of Sound and Vibration*, vol. 39, no. 1, pp. 1–33, 1975.

[14] J.-L. Auriault, C. Boutin, and C. Geindreau, *Homogenization of Coupled Phenomena in Heterogenous Media*, vol. 149, John Wiley & Sons, 2010.

[15] J. Allard and N. Atalla, *Propagation of Sound in Porous Media: Modelling Sound Absorbing Materials 2e*, John Wiley & Sons, 2009.

[16] COMSOL Multiphysics, *Acoustics Module User Guide Version 4.2. Users Manual*, COMSOL AB, Stockholm, 2011.

[17] G. Kirchhoff, "Ueber den Einfluss der Wärmeleitung in einem Gase auf die Schallbewegung," *Annalen der Physik und Chemie*, vol. 210, no. 6, pp. 177–193, 1868.

[18] John William Strutt Baron Rayleigh, *Theory of Sound*, Macmillan and co., London, 1877.

[19] G. P. Ward, R. K. Lovelock, A. R. J. Murray, A. P. Hibbins, J. R. Sambles, and J. D. Smith, "Boundary-layer effects on acoustic transmission through narrow slit cavities," *Physical Review Letters*, vol. 115, no. 4, article 044302, 2015.

[20] S. Y. Song, X. H. Yang, F. X. Xin, S. W. Ren, and T. J. Lu, "Modeling of roughness effects on acoustic properties of micro-slits," *Journal of Physics D: Applied Physics*, vol. 50, no. 23, article 235303, 2017.